JOURNAL OF SPACECRAFT AND ROCKETS
Vol. 36, No. 4, July–August 1999

Optimal Artificially Blunted Leading-Edge Airfoils for Enhanced Aerothermodynamic Performance

Anurag Gupta* and Stephen M. Ruffin†
Georgia Institute of Technology, Atlanta, Georgia 30332-0150

An artificially blunted leading-edge concept that can be applied to the blunted leading edges of vehicles in hypervelocity flight for drag reduction is described. By creating a channel sized to choke at the design condition, most of the wall on which the stagnation region pressure acts is removed; this results in significantly reduced total drag. To evaluate the effectiveness of airfoils employing this concept in achieving low drag without paying any penalties in other areas like lifting capacity, heating rates, or enclosed volume, the design space is characterized comprehensively using multidisciplinary design optimization techniques. Response surface methods are used to search the design space efficiently for such airfoils designed to operate at Mach 4 and 12-km altitude. The results from a designed set of numerical experiments, i.e., Navier–Stokes simulations, are used to create analytical models for force coefficients and peak heat transfer rates. These nonlinear models are then used to generate an optimal channel airfoil design. The performance predicted by the models is verified by Navier–Stokes solutions to validate the optimal design and to evaluate the efficacy of the concept evaluation technique. The optimal airfoil had a 19% lower c_d and a lower peak heat transfer rate while providing the same c_l and enclosed area as the baseline (4% thick) blunted diamond airfoil. The models were accurate to within 5% of the calculated values and demonstrated the ability to smoothly capture trends in system responses while filtering out numerical noise.

Nomenclature

c = chord length, m
c_d = coefficient of drag, with reference area $= (c \times 1)$
c_l = coefficient of lift, with reference area $= (c \times 1)$
h = altitude, km
L/D = lift-to-drag ratio
M_∞ = freestream Mach Number
q_∞ = freestream dynamic pressure
r_n = nose radius of airfoil, m
$r_{n,l}$ = radius of the lip at the channel entrance, m
S_{enc} = area enclosed by airfoil surface, m^2
T_{wall} = temperature of isothermal wall, K
t/c = thickness-to-chord ratio of airfoil
t_c = channel thickness, m
α = angle of attack, deg
θ = angle of inclination of the lower channel wall, deg

Introduction and Overview of Concept

THE range, payload mass fractions, economic feasibility, and other performance criteria of high-speed aerospace vehicles currently being studied (like the high-speed civil transport, launch vehicles, and planetary entry vehicles) are extremely sensitive to aerodynamic drag. A discussion of the effects of drag reduction on such high-speed vehicles is given by Bushnell.[1] Hefner and Bushnell[2] and Jones[3] have also reviewed supersonic drag reduction techniques in the past. Although most of the contemporary drag reduction research has focused on means of reducing the viscous drag, work on the manipulation of high-speed flow features and interactions to reduce drag has been lagging.

The drag on supersonic vehicles can be classified into three categories: 1) skin-friction drag, 2) drag due to lift, and 3) zero-lift bluntness (thickness-wave) drag, which is the wave drag due to the vehicle's thickness and bluntness of the leading and trailing edges in a zero-lift orientation. Leading-edge blunting is necessitated by heating rate limits at high speed, structural/manufacturing reasons, and low-speed aerodynamic performance requirements. This component of drag increases rapidly with freestream Mach number and can be responsible for well over a third of the total vehicle drag. The concept presented focuses primarily on reduction of the zero-lift bluntness drag as a means of reducing the total drag. A reduction of this component of drag and in the total drag can result in increased vehicle range, increased speed, improved fuel efficiency, increased lift/drag ratio, and enhanced performance.

In previous work, Ruffin and Gupta[4] conducted a preliminary investigation of the present drag reduction concept applied to a representative geometry—a blunted diamond airfoil. A range of geometric parameters and supersonic flight conditions were considered so that the aerothermodynamic performance of airfoils employing the present concept could be evaluated. Although the artificially blunted leading-edge (ABLE) concept reduced total drag by over 30 and 20% (for laminar and turbulent flow, respectively) relative to geometries without channels, some geometries considered had higher peak heat transfer rates. The work presented in this paper aims to establish the feasibility of the concept by quantifying the aerothermodynamic performance benefits while operating under other constraints. Multidisciplinary design optimization (MDO) techniques have been used to evaluate the concept over a large design space, to characterize its behavior, and to generate ABLE airfoils that optimize both aerodynamic performance and peak heat transfer rates.

The present concept allows for a hollow channel to be opened at the supersonic leading edges of noses, wings, or other appendages of supersonic and hypersonic vehicles. The channel begins at the leading edge of the airfoil with freestream air flowing passively through the channel and exhausts at the trailing edge. Figure 1 illustrates this concept applied on a blunted symmetric diamond airfoil. When the channel concept is utilized, the vehicle (airfoil) surface that experienced most of the high, near-stagnation pressure is removed and thus leads to lower wave drag. This reduction in sectional drag coefficient can increase cruise efficiency or can be utilized to reduce the amount of wing sweep.

The channel thickness needs to be sufficiently small so that a choked flow condition exists (Fig. 2), a normal shock rests in front of the channel, and the flow enters the channel subsonically. In this case, the flow is decelerated significantly through the shock, and the overall flow structure is similar to that of the no-channel airfoil. If instead the channel is sufficiently large, much of the bow shock is swallowed by the channel—much like a started inlet—and heat transfer rates at the lips increase significantly. Whereas the channel increases the total wetted surface area, the increase in

Received 16 June 1998; revision received 25 September 1998; accepted for publication 29 September 1998.

*Ph.D. Candidate, School of Aerospace Engineering. Student Member AIAA.
†Assistant Professor, School of Aerospace Engineering. Member AIAA.

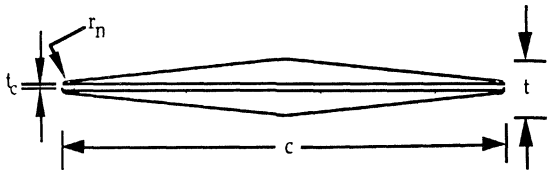

Fig. 1 Schematic of an ABLE airfoil.

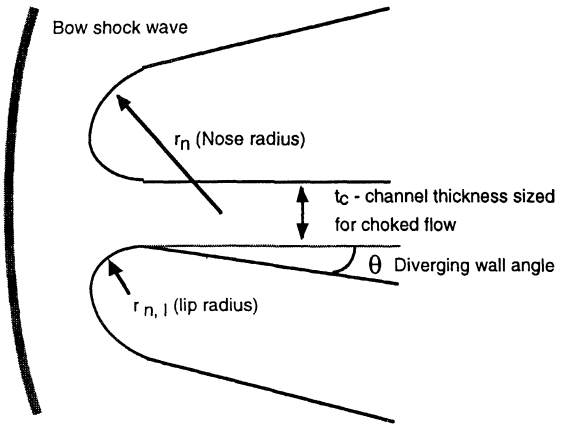

Fig. 2 Schematic of choked flow structure possible at leading edge when channel is utilized.

skin-friction drag can be reduced by maintaining a subsonic flow, and hence a much lower dynamic pressure, through the channel. Overall, utilizing the channel is expected to yield lower wave drag and increased skin-friction drag relative to a no-channel section. The maximum heat transfer rate at the leading edge is a function of the channel thickness, the geometry of the channel entrance (i.e., the nose and channel lip radii), and freestream conditions.

Initial Numerical Results, $M_\infty = 2.4$

The baseline geometry selected is the blunted diamond airfoil because it inherently experiences low inviscid (thickness) wave drag. In the initial proof of concept study, Ruffin and Gupta[4] used as the baseline a no-channel airfoil that was 5% thick, with a chord length of 1.0 m and a nose radius of 5 mm; channels of sizes from 2 to 16 mm were created by carving away a slice about the centerline of the baseline geometry. Different channel entrance shapes (sharp vs rounded lips) and channel wall angles were tested. The following terminology is used to describe the various airfoil geometries: no-channel (baseline) airfoil (NC); round-nose channel airfoil (RNC); round-nose straight channel (RNSC); round-nose diverging channel (RNDC); sharp-nose channel (SNC); and sharp-nose straight channel (SNSC) ($r_{n,l} = 0$).

These initial simulations of two-dimensional flow around airfoils with a freestream Mach number of 2.4 and an altitude of 12 km can be thought of as modeling the low supersonic flow around unswept wings or as modeling the flow normal to the leading edge of a hypersonic vehicle with a swept leading edge. Reynolds-averaged Navier–Stokes (RANS) predictions of aerodynamic and thermal loads on the bodies are obtained using the Generalized Aerodynamic Simulation Program (GASP).[5] This computer code is a well-validated, multizone, finite volume solver. Both laminar simulations and fully turbulent simulations using the Baldwin–Lomax turbulence model were conducted. A comparison of the drag for the baseline NC airfoil and various ABLE airfoils for laminar flow shows that each of the channel airfoils experiences approximately 35% lower total drag relative to the no-channel geometry at a zero-lift condition. For turbulent flow a 14–21% total drag reduction was obtained; use of the channel results in a nearly uniform downward shift in sectional drag coefficient polar as shown in Fig. 3. As the lift generated by the airfoils is unaffected, the maximum lift/drag (L/D) was shown to have increased by approximately 20% for turbulent flow when the channel is utilized.

Two additional findings were developed based on the initial studies. First, it was found that even when the ABLE airfoil had its

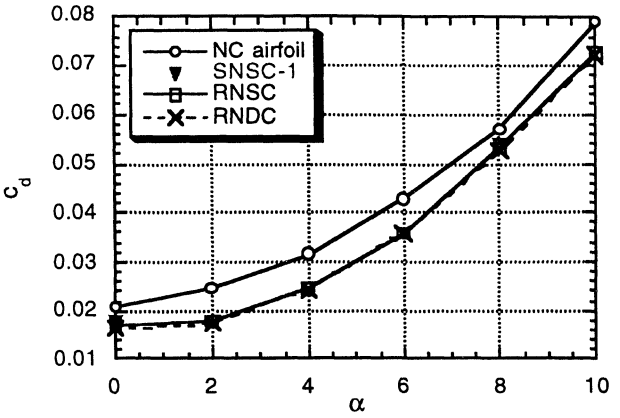

Fig. 3 c_d vs angle of attack for no-channel and ABLE airfoils in fully turbulent flow; $M_\infty = 2.4$ and $h = 12$ km.

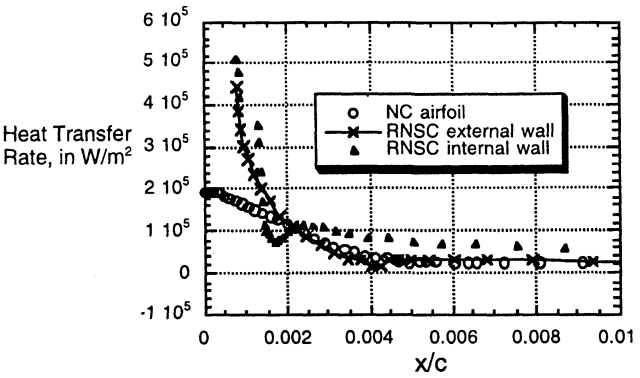

Fig. 4 Computed heat transfer rate near the leading edge for NC and RNSC airfoils in laminar flow; x/c is streamwise distance/chord, $M_\infty = 2.4$, $\alpha = 4$ deg, and $h = 12$ km.

thickness scaled to maintain the same enclosed area as a baseline airfoil, the former had much lower drag. This area enclosed inside an airfoil relates directly to the volume in the wing and is important because it is needed for structural members and/or for fuel storage. Second, although the effective blunt body flow structure reduces the heat transfer relative to a started condition geometry, the channel airfoil still experiences a higher maximum heat transfer rate than the conventional no-channel airfoil when the lip radii are small. For example, Fig. 4 shows that the maximum heat transfer (calculated assuming an isothermal airfoil surface at 300 K) rate for an RNSC airfoil was higher than that for the baseline airfoil when a small lip radius of 0.5 mm was used.

Concept Evaluation and Optimization Methodology

The preliminary analysis explored a limited and distinct set of design points, e.g., sharp vs rounded channel entrance shapes. A larger lip radius would definitely lead to a lower heating rate but what effect would it have on the expected drag reduction? A larger channel size could potentially mean a larger drag reduction depending on the effect of the increased thickness or length resulting from a requirement to maintain enclosed volume. In short, in addition to the effect of each geometric feature, the effect of one on and in conjunction with the other must be accounted for. To address such issues, and to comprehensively assess the possible benefit of the concept, a much larger set of numerical experiments is desired.

Typical conceptual design level analysis tools are generally lower-order methods that use linearized techniques to achieve fast execution. As such, they cannot evaluate radical geometric concepts and configurations whose flowfields are characterized by nonlinear phenomena like the normal shock wave standing off the choked channel. The simplifications in the analysis method also create numerical noise that can cause calculus-based search methods to reach local optima and provide suboptimal answers.[6] Hence it becomes important to not sacrifice the fidelity of the analysis methods during the evaluation phase. For this work, RANS simulations were

deemed necessary to understand the effect of ABLE geometry on the flowfield at different attitudes and to measure force coefficients and peak heat transfer rates accurately.

Given a set of design variables whose ranges are spanned by a chosen number of discrete values, the analysis would have to be repeated for all of the values each variable could reasonably take and at all of the combinations of such possibilities. Such an analysis would be a full factorial experiment. When we consider channel airfoils with a blunted diamond shape as shown in Fig. 1, there are six design variables that can affect aerothermodynamic performance: t/c, r_n, t_c, θ, $r_{n,l}$, and α.

Here the number of numerical experiments required for the full factorial experiment $= L^6$, where $L =$ number of discrete values chosen to discretize each variable range. Obtaining such a large number of Navier–Stokes solutions would be prohibitively expensive in terms of time and resources for a new concept exploration. Hence, in the present study an efficient concept evaluation and optimization methodology based on response surface methods is implemented.

Response Surface Methods

Response surface methods[7] (RSM) are techniques used to find regions of optimality in the design space and to approximate a system response accurately. They provide a structured method of modeling the responses, or outcomes, of an experiment as functions of the independent design variables integrating techniques like design of experiments, regression, and analysis of variances (ANOVA). These response surfaces or equations can have varying degrees of resolution and, once formulated, can be used to identify design drivers and can be used as fast analysis modules, thus simplifying multidisciplinary integration. RSM allows disciplinary codes to be executed by specialists a priori to overall design, rather than by generalists using a monolithic design code.

However, the most significant benefit is that the smooth polynomial models created avoid the problem that numerical noise creates for optimization convergence and reliability even with numerical experiments. Giunta et al.,[8] Balabanov et al.,[9] and Madsen et al.[10] have shown the adverse effect of this noise on optimization and how the application of RSM mitigate its effect. When computer experiments are used, the sources of this numerical noise are typically discretization errors, variation in convergence of iterative solutions, roundoff errors, etc. In addition, the sensitivity of computational fluid dynamics (CFD) results to variations in grid quality, i.e., clustering, skewness, boundary orthogonality, and resolution, is well known. This sensitivity is the primary source of numerical noise even when high-fidelity methods such as RANS simulations are being used for the computational experiments. Regression analysis and ANOVA techniques seek to minimize the effect of this noise, or random error, while building models. These models enhance the chances that the optimizers will find the global minima, regardless of the starting points of the optimization process, and can be used in gradient-based optimizations that would have been impractical to carry out if each function evaluation was a Navier–Stokes solution.

RSM suffers from the curse of dimensionality; i.e., as the number of design variables increases, the number of experiments required to create the model increases to unmanageable levels, especially if the analyses are expensive. For example, a quadratic polynomial with 6 variables has 28 coefficients, one with 10 variables has 66 coefficients, etc., and the number required to fit a reliable model is even greater. Hence, as Myers and Montgomery[7] explain, RSM is typically done in a sequential fashion with screening experiments to identify important factors, to use simpler models to predict directions of improvement, and to move to locations where a higher-order model can be fit over a smaller design volume with fewer variables. The initial screening experiment can also be used for discarding infeasible combinations as demonstrated by Giunta et al.[8] with the variable complexity RSM. For the present concept evaluation, we are interested in identifying trends that will answer questions on the feasibility of ABLE airfoils and in locating ABLE airfoils that meet certain design constraints. Hence a response surface is generated only once to approximate the behavior of the concept over the entire design space.

Design of Experiments

Design of experiments, originally formalized by the British statistician R. A. Fisher in the 1920s, uses statistical techniques to reduce the full factorial experiment to a smaller, yet meaningfully chosen subset. Elements of this array are point designs chosen mathematically to characterize all of the chosen effects of and any required interactions between the design variables. They also avoid biasing the analysis (i.e., being influenced by the level of one design variable), which is typical of a one-at-a-time parametric study.

The accuracy of the response surface approximation and the cost of creating it depend directly on the choice of experimental design. That choice, in turn, needs to provide a good fit of the model to the data and hence depends on the type of response model that is sought. It also has to give sufficient information to allow for the use of statistical quality measures from regression analysis. These needs usually conflict with cost effectiveness, and when the experiments are expensive, as Navier–Stokes simulations are, a compromise between the number of experiments specified and resolution of experimental design is sought. When this happens, saturated or near-saturated designs that have run sizes equal to or just greater than the terms in the expected model are used.

When quadratic effects are expected, or modeled, RSM typically use central composite designs (CCDs) and Box–Behnken designs. CCDs allow for sequential experimentation, with the additional runs needed only after curvature in the response surface has been tested for, and with each factor tested at a maximum of five levels; the Box–Behnken designs are three-level designs that, although more efficient, are not very accurate in predicting responses at extremes of the design space. The characteristics of these designs along with saturated designs like hybrid Koshal designs are presented in detail by Myers and Montgomery.[11] All of the aforementioned designs, however, suffer from one disadvantage—they assume a regularly shaped design space.

When a multivariate system is subject to complex constraints, the design space quickly becomes irregular with infeasible combinations of variable levels distributed throughout. The experimental design problem is now converted to choosing a combination of feasible points that provide an appropriate design. The D-optimality criterion,[12] which seeks to minimize generalized variance of the responses as well as parameter estimates, or more correctly, its maximization, has been a widely used technique for experimental design in irregular design spaces.[8–10,13] The D-optimality criterion allows for sequential experimentation and, being a minimum-variance design, provides robustness to noise in the data. However, it is not designed to minimize the effect of modeling errors, which minimum bias designs do. Recently minimum bias designs have been used in structural optimization[9] and design of aerospike nozzles[14]; although they are significantly more difficult to obtain for irregular spaces, no significant improvements in the performance of optimal designs were found. Hence, a D-optimal experimental design is used for our study.

Regression and Analysis of Variances

The functional relationship between a response y and the independent design variables x_i can be expressed as

$$y = F(x_1, x_2, x_3, \ldots, x_k) + \varepsilon \tag{1}$$

where ε represents the total error, i.e., variability not accounted for by F, and k is the number of design variables affecting the response. RSM seeks to model the unknown function F with a low-order polynomial; we use a second-order model because they are flexible and easy to work with and have been used widely to approximate nonlinearities in system responses. The second-order model can be represented mathematically as

$$\hat{y} = \beta_0 + \sum_{i=1}^{k} \beta_i x_i + \sum_{i=1}^{k} \sum_{j=1}^{k} \beta_{i,j} x_i x_j \tag{2}$$

where the various β are the unknown parameters that need to be estimated. The designed experiment is a table of variable values, with each row representing variable values for each run, called the design matrix ($\boldsymbol{X}$). Then if $\boldsymbol{Y}$ is the vector of measured responses and

β is the coefficient matrix for the response model, the approximation can be represented in matrix form by

$$Y = X\beta + \varepsilon \tag{3}$$

Regression analysis is a branch of statistical model building that uses response data collected at different points to do so; here, linear regression analysis and, more specifically, the least-squares method are used to estimate the coefficients, which can be represented by

$$\beta = (X^T X)^{-1} X^T Y \tag{4}$$

The coefficients corresponding to insignificant effects are dropped to simplify the response equation. The second-order response models provide a quick way to calculate lift and drag coefficients and the maximum heat transfer rate for any channeled diamond airfoil as a function of α and airfoil geometry. Similar models can be generated for any other parameter of interest.

There are several techniques to choose the best model or to refine a regression model. Detailed explanations are given in Refs. 7 and 15. The model needs to have an accurate predictive capability and its coefficients need to be estimated with a good degree of confidence. As such the effect of each term in the model has to be tested. Regression analysis and ANOVA provide measures of quality to guide the selection of terms in the final model.

The t statistic of a coefficient is the ratio of its value to an estimate of the standard error of that coefficient. Terms with relatively low t statistic can be removed to avoid the dangers of overfitting and to improve the prediction accuracy. The F ratio of a factor is the variance of the factor divided by the error variance; if its value is greater than that expected from chance alone, the effect is deemed significant. A similar test can be applied to the entire model. The overall quality of the response model can be measured using the following metrics.

1) The term R^2 quantifies the proportion of variation around the mean explained by the model. The R^2 value always goes up as terms are added to a model.

2) The term R^2_{adj} provides an unbiased estimate of the variation accounted for and adjusts R^2 to make it more comparable over models with different numbers of parameters. It can be used to guide model refinement; when unnecessary terms are added, the value of R^2_{adj} often decreases.

3) Residual errors in the least-squares fit for the model measure error due to both improper modeling and numerical noise. These are expressed as percentages of the total variation in each model.

Experimental Design

For this concept evaluation study, the operational conditions were specified as Mach 4.0 flight at a 12-km altitude. The baseline airfoil chosen was a 4% thick, no-channel airfoil with a nose radius of 10 mm and a chord length of 2 m operating at $\alpha = 4$ deg. The objective was to obtain an ABLE derivative that reduced drag while attaining the same lift coefficient and the same or lower peak heat transfer rate relative to the baseline. To ensure that the comparison between the NC and ABLE airfoils was fair, no loss of enclosed area was tolerated. The chord c of the ABLE airfoils was scaled to maintain the same S_{enc} while nondimensionalizing the other design variables with c. Thus the channel airfoils have a larger thickness t than the corresponding no-channel airfoils to maintain the same t/c. Certain constraints had to be met to ensure that the candidate geometries were geometrically and physically viable. From geometry,

$$r_n \le t/2, \qquad r_{n,l} \le \tfrac{1}{2}[r_n - (t_c/2)] \tag{5}$$

The maximum channel size was limited by the requirement to keep the flow inside it choked and was a function of the freestream Mach number and the nose radius. For Mach 4.0, this relationship was approximated by another response equation:

$$t_c \le 0.6 r_n - 0.0005 \tag{6}$$

These constraints were used to determine ranges and as filters while generating the candidate geometries. Table 1 lists the six design variables and their ranges. A negative θ corresponds to a converging channel with only the lower channel wall slanted up. The range for each variable was discretized into a fine grid and a full factorial array was set up. The filters removed unrealistic combinations to create a final set made up of 6480 feasible airfoil geometries. The dimensional variables were nondimensionalized with c, and this set of candidate geometries was used to pick the D-optimal set.

Table 1 Discretization of variable ranges for generation of candidate geometries

Variable	Range	Levels
t/c, %	4–8	5
r_n, m	0.01–0.08	7
t_c, m	0.00–0.0475	9
θ, deg	−0.1–+0.1	3
$r_{n,l}$, m	0.00–0.016	6
α, deg	0.00–25.0	10

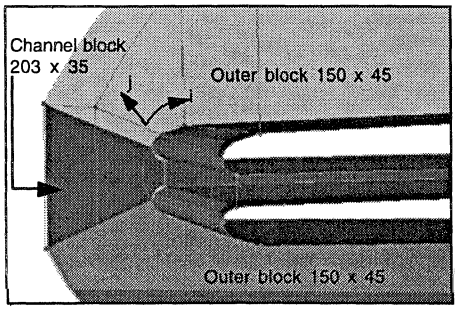

Fig. 5 Schematic depicting multiblock grid boundaries of ABLE airfoil grids used in design study.

A postulated model should reflect an appreciation of the physical relationships between responses and variables. In addition to the factors mentioned, the choice of the second-order model and of the form in which the design variables x_i were used was based on known relationships for responses such as the coefficients of lift, drag, and heating rates such as

$$C_l \sim f(\alpha, \alpha^2), \qquad C_d \sim f(\alpha, \alpha^2)$$

$$\dot{q} \sim f\left(1/r_n^{0.5}\right), \qquad C_d \sim f(t/c)^n$$

where the exponent $n = 2$ for a sharp diamond airfoil (from inviscid considerations). The minimum number of runs required to fit a given quadratic model, i.e., a saturated design of experiments, is given by $0.5(k+1)(k+2)$, where $k =$ number of design variables. With 6 variables, 28 runs were obtained. As mentioned before, the D-optimal design has a tendency to choose experiments on the boundaries of the design space. As such, the set of experiments obtained did not have a sufficient number of evaluations in the midrange of design variables like α. To ensure that the designed set characterized the complete range of α and thus to reduce the bias of the experimental design, a few midrange levels were chosen iteratively to minimize the negative impact on the D-optimality criterion. The final designed set of experiments is listed in Table 2.

Numerical Experiments: CFD Analysis

Structured grids with approximately 20,000 grid points per two-dimensional plane were constructed for each of the geometries using GRIDGEN.[16] Whereas the NC grids utilized a single block grid, the ABLE geometries needed a multiblock grid (see Fig. 5). Initial algebraic grids were generated and then refined using the elliptic solver to provide orthogonality at the walls. To ensure an accurate capture of viscous effects, approximately 15 points were placed inside the boundary layer. From previous experience, a grid with 45 nodes in the direction normal to the wall with the first node 0.05 mm away from the wall gave sufficiently accurate answers[4] and was economical enough to be used in a concept evaluation study. A grid-refinement study was also carried out to verify the validity of the choice of grid dimensions. Fine grids were created with twice the number of points in the direction normal to the wall by inserting grid nodes between every pair of nodes in the original

Table 2 Designed set of experiments and aerothermodynamic responses from the Navier–Stokes solutions[a]

Run no.	t/c	$\sqrt{(r_n/c)}$	t_c/c	θ	$r_{n,l}/c$	α	c_l	c_d	$\dot{q}_{inv}$
1	0.04	0.07071	0	0	0	25	0.55470	0.27716	0.398
2	0.06	0.17	0	0	0	25	0.52095	0.32039	0.770
3	0.08	0.07071	0	0	0	0	0.00000	0.02067	0.468
4	0.08	0.13	0	0	0	20	0.40618	0.19840	0.655
5	0.08	0.17	0	0	0	0	0.00000	0.07775	1.083
6	0.04	0.11	0.005	−0.1	0.004	0	0.00000	0.03278	0.435
7	0.04	0.13	0.005	−0.1	0	25	0.54185	0.29462	——
8	0.04	0.13	0.005	0.1	0.006	25	0.53908	0.29385	0.536
9	0.04	0.13	0.005	0.1	0	0	0.00000	0.03952	——
10	0.05	0.15	0.005	−0.1	0.008	12	0.20994	0.10353	0.534
11	0.06	0.17	0.005	−0.1	0	0	0.00000	0.06953	——
12	0.06	0.17	0.005	0.1	0.006	0	0.00000	0.07013	0.360
13	0.07	0.11	0.005	−0.1	0	0	0.00000	0.03250	——
14	0.07	0.11	0.005	0.1	0.004	0	0.00000	0.03015	0.329
15	0.08	0.11	0.005	−0.1	0.004	15	0.28889	0.11419	0.523
16	0.08	0.11	0.005	0.1	0	25	0.55065	0.29254	——
17	0.08	0.15	0.005	0	0.008	25	0.52931	0.30851	0.470
18	0.08	0.17	0.005	0.1	0	15	0.27844	0.14837	——
19	0.08	0.17	0.005	−0.1	0.006	25	0.53275	0.32082	0.364
20	0.05	0.15	0.012	0.1	0.008	0	0.00000	0.04980	0.224
21	0.08	0.15	0.012	0	0.004	12	0.22457	0.09228	0.418
22	0.06	0.17	0.016	−0.1	0	5	0.08528	0.06453	——
23	0.06	0.17	0.016	−0.1	0.008	25	0.53474	0.30719	0.485
24	0.06	0.17	0.016	0.1	0	25	0.54654	0.30496	——
25	0.08	0.17	0.016	−0.1	0	25	0.54276	0.31046	——
26	0.08	0.17	0.016	−0.1	0.008	0	0.00000	0.05753	0.365
27	0.08	0.17	0.016	0.1	0	0	0.00000	0.05445	——
28	0.08	0.17	0.016	0.1	0.008	15	0.28449	0.13125	0.505

[a]All calculations were at $M_\infty = 4.0$, $h = 12$ km, and $T_{wall} = 800$ K.

grid. GASP solutions with the same input parameters on these fine grids showed that c_l and c_d values using the coarser grid were off by 0.96 and 1.95%, respectively. Thus, we estimate that the calculated lift and drag results are within an acceptable 2% of those obtained from very fine grid solutions. Hence all geometries in the present study were gridded to this same resolution.

It is important to remember that the use of the elliptic solver and variations in actual geometry create small variations in off-the-wall spacing that introduce noise in the eventual responses, i.e., force coefficients and heat transfer rates. The heat transfer characteristics, being local quantities rather than obtained by integration over the entire geometry, are especially sensitive to variations in grid spacing and skewness. To capture the relative variations in thermal loading due to geometry and flowfield changes accurately, a consistent off-the-wall grid spacing was enforced on all grids.

At freestream conditions for a 12-km altitude and a Mach 4 speed, the flow was assumed to be thermodynamically frozen. The Reynolds number per unit length was about 25.9×10^6/m for the freestream and varied from about 6×10^6/m to 15×10^6/m for the internal channel flow; hence the fully turbulent flow assumption is reasonable. RANS simulations were performed using GASP for each geometry. The third-order upwind-biased Roe's flux difference splitting scheme in conjunction with the min-mod limiter was used. Turbulence was modeled using the algebraic Baldwin–Lomax model. The airfoil walls were treated as isothermal surfaces at a temperature of 800 K; for a detailed analysis of the thermal loads of the kind needed for detailed/hardware design, a conjugate heat transfer analysis would be required. The external flow and internal flow in the channel were solved in a fully coupled fashion. The two-factor approximate factorization method was used for time integration. Although all simulations assumed a steady-state simulation, a few geometries were also solved in a time-accurate mode to check for unsteady phenomena like bow shock oscillation in the presence of the choked channel; none were observed. Convergence was declared when residuals went down by four orders of magnitude; when that criterion was not met, calculations were stopped when the responses reached a steady value.

The flowfield over an RNC airfoil is shown in Figs. 6–8. The single bow shock structure and the creation of the effective blunt body due to the choked channel are presented via a Mach distribution in Fig. 6. The overall flow structure with the leading-edge bow

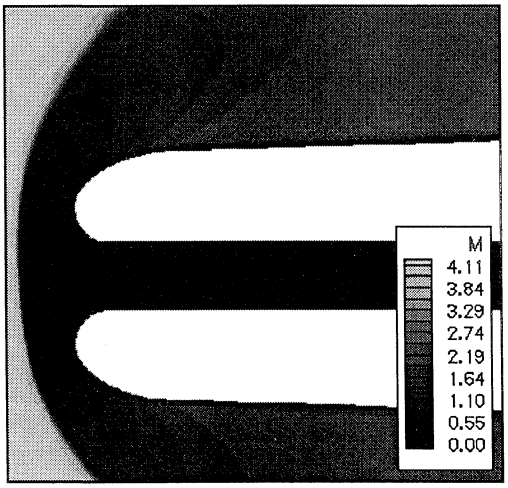

Fig. 6 Mach number distribution at the leading edge of an RNC airfoil; $M_\infty = 4.0$, $\alpha = 4$ deg, and $h = 12$ km.

shock, expansions at midchord, and consequent recompression at the trailing edge is similar to that over a no-channel airfoil and presented in Fig. 7. An interesting feature in this flowfield is the channel exhaust (Fig. 8), which behaves similarly to an underexpanded high-pressure jet. This jet's potential use for directional control or other types of flow control/modification is currently being investigated in related research.

Results: Response Surfaces

Lift and drag coefficients as well as the maximum heat transfer rate on the airfoil surface were calculated. These form the responses for each of the experiments. The aerodynamic coefficients and peak heat transfer rates are presented in Table 2. As the force coefficients are nondimensional, the response equations for c_l and c_d will be in terms of nondimensional design variables. The peak heat transfer rates are dimensional, and so the quantities in the model for heat transfer rates are dimensional. There are three distinct types of airfoils in the data set—NC, SNC, and RNC. Single models for the

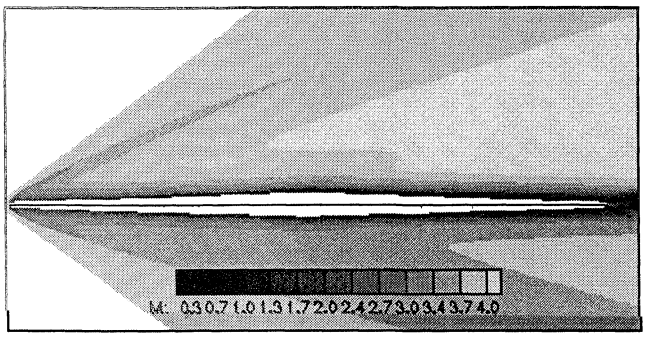

Fig. 7 Overall flow structure for an RNC airfoil: Mach number distribution at $M_\infty = 4.0$, $\alpha = 4$ deg, and $h = 12$ km.

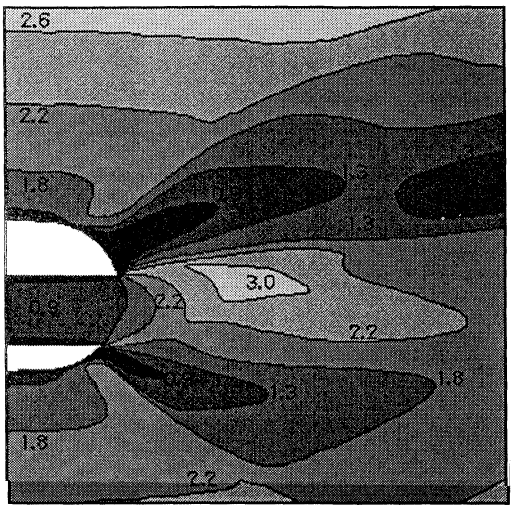

Fig. 8 Flow structure at trailing edge of an RNC airfoil: Mach number distribution at $M_\infty = 4.0$, $\alpha = 4$ deg, and $h = 12$ km.

force coefficients can be created as the transition from a no-channel airfoil to a channeled airfoil can be specified as the zeroing of t_c and setting $r_n = r_{n,l}$. Because the creation of a lip changes the heat-loading characteristics of the airfoil drastically, the heat transfer rates for no-channel and channeled airfoils had to be modeled separately. Although SNC airfoils were part of the data set, we decided to exclude them from forming the basis of the heating rate model because a practical ABLE airfoil would never have a sharp nose and, theoretically, the peak heating rate at a sharp nose is infinity. This made the underlying data set very small and significantly impacted the model fitting. Also, to obtain a well-behaved polynomial, the actual quantity being modeled, where $\dot{q}_{\max}$ is in watts per square meter, is

$$\dot{q}_{\text{inv}} = \frac{1.0e^5}{\dot{q}_{\max}}$$

Initial models with all 28 effects (terms of the polynomial) are created for the force coefficients. Backward elimination of the most uncertain regressor based on the t statistic and F ratio is used to come up with the best subset of parameters. After a term is removed, improvement in R^2_{adj} and a lower rms error indicate better fit quality and vice versa. At the same time, the degrees of freedom, or the number of points over which the model is tested, go up to improve the certainty associated with coefficient estimation. Visual tools like the Bayes plot of normalized estimates and interaction plots are also used to gauge the relative significance of effects. The aim is to create a model with the minimum number of well-estimated terms and the best R^2 and R^2_{adj} values. Single polynomial models for lift and drag coefficients for the entire design space spanning NC, SNC, and RNC airfoils were created to a surprisingly high quality as they are able to saddle smoothly the variations due to changing airfoil types; with only 8 and 10 terms in the model (excluding the intercept), the model has sufficient degrees of freedom, R^2_{adj} values $\sim \mathcal{O}(0.999)$, and rms errors smaller than 0.5%. These models, called response surface equations (RSEs), can be written out as

$$\begin{aligned} c_l &= 0.01768 + 0.0152\alpha + 0.00026\alpha^2 - 0.0099(t/c) \\ &\quad - 0.14532\sqrt{r_n/c} + 0.7282(t_c/c) - 0.6716(r_{n,l}/c) \\ &\quad - 0.01036\theta(t/c) + 0.05036\theta\sqrt{r_n/c} \\ c_d &= 0.0738 - 0.00207\alpha + 0.00048\alpha^2 + 0.03125(t/c) \\ &\quad + 0.07646\sqrt{r_n/c} - 1.0336(t_c/c) - 0.34153(r_{n,l}/c) \\ &\quad + 0.38605\theta(t/c) - 0.23356\theta\sqrt{r_n/c} \\ &\quad + 1.773(r_n/c) + 35.585(r_{n,l}/c)^2 \end{aligned}$$

It is important to recall that these models are accurate and valid only in the ranges of design variables used to generate them. For both c_l and c_d, the α and α^2 terms have an expected strong effect in the model. The RSEs also point toward the decrease in c_d due to the presence of the channel via the negative coefficient of the t_c term as well as the dependence of the effect of angling the wall θ on the levels of other design variables. The characterization of the latter effect is important; we expected that creating a divergent channel would allow the high-pressure flow in the channel to exert a small axial force in the direction of motion to reduce drag. The effect of angling the wall also opens up the possibility of tailoring the channel geometry to obtain favorable characteristics.

Creating the RSEs for peak heat transfer rates was constrained by paucity of data for NC and RNC airfoils—5 and 13 data points, respectively. The $\dot{q}_{\max}$ value depends on the leading-edge geometry and thus is fairly independent of the airfoil thickness and channel wall angle. This reduction in the number of independent variables in the model from 6 to 2 (α and r_n for NC airfoils) and 4 (α, r_n, $r_{n,l}$, and t_c for RNC airfoils) mitigates this problem and allows us to set up smaller and simpler starting models. Stepwise regression methods create reduced models by adding terms sequentially to a simple starting model (forward regression) or by reducing from the complete model (backward regression) until a specified quality of fit is achieved. The mixed stepwise regression method applies backward regression to eliminate a term and then tries a forward regression with all excluded terms. This method has been shown to provide good reduced models[17] and is used here to create intermediate response surfaces. The quality of fits and certainty of the parameter estimates are analyzed again—the insignificant terms are dropped and expected physical interaction terms added to see whether they add to the predictive accuracy of the model.

The final models for peak heat transfer rates over NC and RNC airfoils have three and seven terms, respectively, excluding the intercept terms. The NC model airfoil has very good R^2_{adj} (0.999) and error values (0.73%) but has only one degree of freedom. As mentioned before, the peak heating rate is very sensitive to numerical noise in the CFD solution, which creates a large spread in the data. These factors combine to create the low R^2 and R^2_{adj} values of 0.916 and 0.82, respectively, for the RNC airfoil's response surface. The RSEs are given as

$$\dot{q}_{\text{inv}}(\text{NC}) = 0.0296 + 0.004\alpha + 6.19\sqrt{r_n} - 0.098\alpha\sqrt{r_n}$$

$$\begin{aligned} \dot{q}_{\text{inv}}(\text{RNC}) &= 0.782 + 0.02\alpha + 74.75r_{n,l} - 58.042r_n \\ &\quad - 9508.42t_c^2 - 1617.68r_n r_{n,l} - 0.00072\alpha^2 + 6883.02r_n t_c \end{aligned}$$

As expected, for the NC geometry, the reciprocal of the maximum (stagnation point) heating rate is dominated by the $\sqrt{r_n}$ term. The statistical quality measures of all of the RSEs are summarized in Table 3.

Results: Optimization and Verification

The aim of the optimization phase is to generate an ABLE design that provides a better aerodynamic performance than the baseline airfoil operating at $\alpha = 4$ deg and Mach 4.0 without sacrificing performance in handling thermal loads or packaging. It should be noted that for the design space in consideration this baseline is

Table 3 Statistical quality measures of response surfaces

Response	Measure			
	R^2	R^2_{adj}	rms error, %	Terms[a]
c_l	0.999	0.999	0.49	8
c_d	0.999	0.999	0.35	10
$\dot{q}_{inv}$(NC)	0.999	0.999	0.73	3
$\dot{q}_{inv}$(RNC)	0.925	0.821	4.00	7

[a]Number of terms in model excluding the intercept.

Table 4 Baseline and optimal ABLE airfoil geometries

Variable	t/c, %	r_n, m	t_c, m	θ, deg	$r_{n,l}$, m	Chord, m
Baseline	4	0.01	——	——	——	2.0
Optimal	4	0.01	5.5×10^{-3}	0.1	2.72×10^{-3}	2.275

the thinnest and sharpest possible geometry; hence the minimum drag no-channel airfoil. The characteristics of the baseline airfoil are predicted using the response surfaces and also are verified by calculating a turbulent flow, Navier–Stokes solution.

The response models obtained for the channel airfoils are coupled with a gradient-based optimizer, the commercially available Design Optimization Tools.[18] For this constrained problem, the sequential quadratic programming method is used. The optimization problem is set up as a drag minimization problem, whereas the geometric and physical conditions used to select viable channel geometries are formulated into constraints. These include the scaling of the chord to maintain the same enclosed area as the baseline. The design is also constrained to achieve at least the same c_l as the baseline and to not have a higher peak heat transfer rate. The ranges of design variables supplied are the same as those used to set up the designed experiments.

The aerothermodynamic optimization of the channel airfoil is completed in about 63 function calls and a few seconds on a workstation. All of the constraints are met, and the optimization process drives the design to the lower bounds of the thickness and nose radius ranges; all of these trends match those expected from a drag minimization process, i.e., toward a thinner airfoil with a sharper nose. The effect of the interactions between θ and r_n, and t and t_c, on c_d and c_l captured in the RSE drives the design toward the upper bounds of the channel wall divergence angle range. The design variable values for the optimized ABLE airfoil are presented in Table 4. The predicted performance of the optimal ABLE airfoil now needs to be verified with a CFD solution.

With these values, a new multiblock grid is generated using the same grid spacing off the wall and topology as the geometries from the designed experiment. A RANS calculation with the same parameters as before is completed for the flow around the optimal geometry at Mach 4, 12-km altitude, and $\alpha = 4$ deg. The effective blunt body flow sturcture limits the peak heating rate for the optimal airfoil to be 15% lower than that of the baseline airfoil. Figure 9 compares the heating rates in the lower leading-edge region of both the baseline NC and the optimal ABLE airfoil.

Although the calculation satisfies the lift and heating rate constraints, overall drag is reduced by 19%. Note that the optimal ABLE airfoil was scaled to maintain S_{enc}, penalizing its drag performance by extra thickness and a larger wetted surface area. Even if a small loss of S_{enc} could be tolerated, the percentage drag reduction would go up.

Table 5 compares the response surfaces predicted and the Navier–Stokes calculated force coefficients and peak heating rates for the baseline NC airfoil. As expected from the good quality measures of force coefficient models, the calculated lift and drag coefficients are in very good agreement with the predicted values. However, the peak heating rate is underpredicted by about 12%; this is because of the paucity of data points to create the baseline heating rate RSE accurately. To gauge the accuracy of the response surface predictions for the optimal ABLE airfoil, they are compared with calculated Navier–Stokes values in Table 6. As expected from the

Table 5 Comparison of predicted (response surface equation) and calculated (Navier–Stokes simulation) loads for baseline airfoil at $M_\infty = 4.0$, $\alpha = 4$ deg, $h = 12$ km, and $T_{wall} = 800$ K

Response	Predicted	Calculated	Accuracy,[a] %
c_l	0.0727	0.0703	+3.41
c_d	0.0215	0.0214	+0.46
$\dot{q}_{max}$, W/m^2	2.19e+5	2.4e+5	−11.93

[a]Accuracy = 100 × (calculated − predicted)/(calculated).

Table 6 Comparison of predicted (response surface equation) and calculated (Navier–Stokes simulation) loads for the optimal ABLE airfoil at $M_\infty = 4.0$, $\alpha = 4$ deg, $h = 12$ km, and $T_{wall} = 800$ K

Response	Predicted	Calculated	Accuracy,[a] %
c_l	0.07405	0.0716	+3.42
c_d	0.01806	0.0174	+4.03
$\dot{q}_{max}$, W/m^2	1.92e+5	2.03e+5	−5.42

[a]Accuracy = 100 × (calculated − predicted)/(calculated).

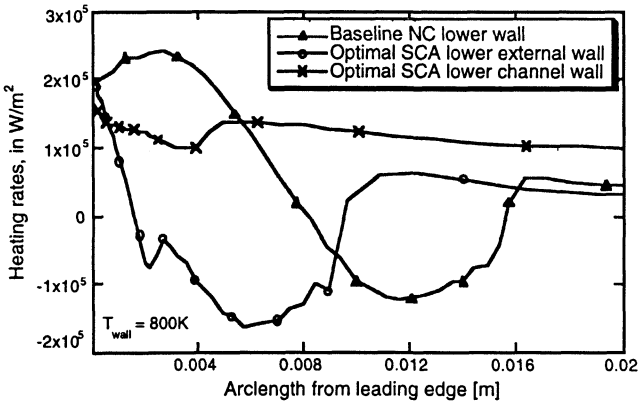

Fig. 9 Leading-edge heating rates comparison at $M_\infty = 4.0$, $\alpha = 4$ deg, and $h = 12$ km flow condition; baseline NC vs optimal ABLE airfoil ($T_{wall} = 800$ K; $\dot{q} > 0$ indicates heat transfer to airfoil).

statistical quality of the RSE, the c_l and c_d predicted values are in good agreement with those obtained by a CFD solution. Although the statistical quality of the maximum heat transfer rate RSE was not exceptional, its prediction was off from the calculated result by only 5.4%. Thus, although noise in the heating rate response causes the low R^2 numbers, the overall shape of the response is accurately captured by the smooth RSE. The difference between the predicted and calculated values is consistent with the estimates of accuracy from the grid sensitivity study. Thus, the RSEs are able to filter out the noise to provide accurate predictions.

Conclusions

A supersonic channel airfoil concept that can be applied to the leading edges of wings, tails, fins, struts, and other appendages of aircraft, atmospheric entry vehicles, and missiles in high-speed flight has been described. It is designed to be beneficial at conditions in which the leading edge is significantly blunted and the Mach number normal to the leading edge is supersonic. With a sufficiently small channel, a normal shock exists in front of the leading edge, thus creating a choked entrance condition. The concept reduces total drag and increases L/D relative to geometries without channels.

An efficient aerothermodynamic design methodology using MDO techniques was set up and implemented. An extensive evaluation of the effect of various geometric (design) variables on the aerothermodynamic efficiency of the concept was conducted using design of experiments. The concept's performance was characterized and modeled as nonlinear, second-order equations using a response surface methodology. A baseline 4% thick blunted diamond airfoil operating at Mach 4 and 12-km altitude was chosen, and the design task was to create an optimal channel airfoil geometry that would minimize drag while not exceeding the maximum heating rate of the baseline and still meet the same lift requirement. The response surfaces were coupled to a gradient-based optimizer, and

an optimal ABLE geometry was obtained. Navier–Stokes solutions were calculated for the baseline and the optimized airfoil to verify the accuracy of the response surface predictions. This optimized airfoil demonstrated a drag coefficient reduction of 19% while easily meeting the lift, heat transfer, and enclosed area constraints. The effectiveness of the polynomial models in smoothing out the numerical noise in the CFD analysis to give accurate predictions was also established. The models and the consequent optimization process point toward the potential to tailor the internal channel wall geometry to enhance performance.

Acknowledgments

Computational support was provided by the Pittsburgh Supercomputing Center in Pittsburgh, Pennsylvania, and the High Performance Computing group and facilities at the Georgia Institute of Technology. The authors wish to acknowledge gratefully the support and guidance of John Olds for the optimization effort. The JMP® Statistical Analysis software was used for the design of experiments and model fitting effort.

References

[1]Bushnell, D., "Supersonic Aircraft Drag Reduction," AIAA Paper 90-1596, June 1990.

[2]Hefner, J. N., and Bushnell, D. M., "An Overview of Concepts for Aircraft Drag Reduction," AGARD Rept. 654, June 1977, pp. 1-1–1-30.

[3]Jones, R. T., "Aerodynamic Design for Supersonic Speeds," *Advances in Aeronautical Science*, Vol. 1, No. 1, 1959, pp. 34–52.

[4]Ruffin, S. R., and Gupta, A., "Supersonic Channel Airfoils for Reduced Drag," AIAA Paper 97-0517, Jan. 1997.

[5]McGrory, W. D., Slack, D. C., Applebaum, M. P., and Walters, R. W., "GASP Version 3, The General Aerodynamic Simulation Program—User's Manual," AeroSoft, Inc., Blacksburg, VA, May 1996.

[6]Giunta, A. A., Dudley, J. M., Narducci, R., Grossman, B., Haftka, R. T., Mason, W. H., and Watson, L. T., "Noisy Aerodynamic Response and Smooth Approximations in HSCT Design," AIAA Paper 94-4376, Sept. 1994.

[7]Myers, R. H., and Montgomery, D. C., *Response Surface Methodology: Process and Product Optimization Using Designed Experiments*, Wiley, New York, 1995, pp. 2–12.

[8]Giunta, A. A., Balabanov, V., Haim, D., Grossman, B., Mason, W. H., Watson, L. T., and Haftka, R. T., "Wing Design for a High Speed Civil Transport Using a Design of Experiments Methodology," AIAA Paper 96-4001, Sept. 1996.

[9]Balabanov, V., Kaufman, M., Knill, D. L., Haim, D., Golovidov, O., Giunta, A. A., Haftka, R. T., Grossman, B., Mason, W. H., and Watson, L. T., "Dependence of Optimal Structural Weight on Aerodynamic Shape for a High Speed Civil Transport," AIAA Paper 96-4046, Sept. 1996.

[10]Madsen, J., Shyy, W., Haftka, T., and Liu, J., "Response Surface Techniques for Diffuser Shape Optimization," AIAA Paper 97-1801, June 1997.

[11]Myers, R. H., and Montgomery, D. C., *Response Surface Methodology: Process and Product Optimization Using Designed Experiments*, Wiley, New York, 1995, pp. 279–373.

[12]St. John, R. C., "D-Optimality for Regression Designs: A Review," *Technometrics*, Vol. 17, No. 1, 1975, pp. 15–23.

[13]Roux, W. J., Stander, N., and Haftka, R. T., "Response Surface Approximations for Structural Optimization," AIAA Paper 96-4042, Sept. 1996.

[14]Simpson, T. W., "Comparison of Response Surface and Kriging Models in the Multidisciplinary Design of an Aerospike Nozzle," NASA CR-206935, Feb. 1998.

[15]Box, G. E. P., Hunter, W. G., and Hunter, J. S., *Statistics for Experimenters: An Introduction to Design, Data Analysis, and Model Building*, Wiley, New York, 1978, pp. 453–535.

[16]Steinbrunner, J. P., Chawner, J. P., and Fouts, C. L., "The Gridgen 3D Multiple Block Grid Generation System," Vols. 1 and 2, Wright Research and Development Center, WRDC-TR-90-3022, Wright–Patterson AFB, OH, Feb. 1991.

[17]Venter, G., Haftka, R. T., and Starnes, J. H., Jr., "Construction of Response Surfaces for Design Optimization Applications," AIAA Paper 96-4040, 1996.

[18]*DOT Users Manual, Version 4.0*, Vanderplaats, Miura, and Associates, Inc., Goleta, CA, 1993, pp. 20–35.

J. R. Maus
Associate Editor